Journal of Materials Chemistry C

Accepted Manuscript

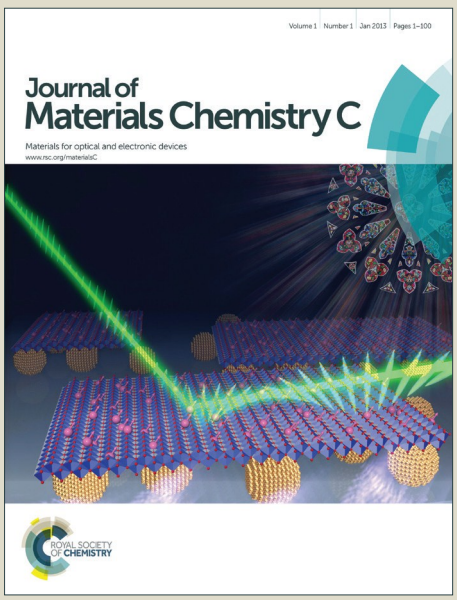

ROYAL SOCIETY OF CHEMISTRY

www.rsc.org/materialsC

Double-side responsive polymer near-infrared photodetectors with transfer-printed electrode

Sixing Xiong,[1] Jinhui Tong,[1] Lin Mao,[1] Zaifang Li,[1] Fei Qin,[1] Fangyuan Jiang,[1] Wei Meng,[1] Tiefeng Liu, [1] Weiwei Li[2,]* and Yinhua Zhou[1,]*

1. Wuhan National Laboratory for Optoelectronics, School of Optical and Electronic Information, Huazhong University of Science and Technology, Wuhan 430074, China

**E-mail: yh_zhou@hust.edu.cn* (Y.H.Z.)

2. *Beijing National Laboratory for Molecular Sciences, CAS Key Laboratory of Organic Solids, Institute of Chemistry, Chinese Academy of Sciences, Beijing 100190, P. R. China.*

**E-mail: liweiwei@iccas.ac.cn* (W.W.L.);

Abstract

Low dark current is critical to realize high-performance near infrared organic photodetectors (NIR-OPDs). In general, organic photodetectors (OPDs) are with vacuum-deposited metals as the top electrode. The deposition of such metal would inevitably form doping to the organic active layer and thus yields high dark current. Here, we employ transfer-printed conducting polymer (tp-CP) as the top electrode instead of the vacuum-deposited metal electrode. The photodetector with tp-CP electrode exhibits over two orders of magnitude lower dark current density than the device with the vacuum-deposited metal electrode. The photodetector with tp-CP electrode displays a responsivity of 0.37 A/W at 850 nm and a low dark current density of 3.0 nA/cm^2 at -0.2 V based on a near-infrared (NIR) active layer of PMDPP3T:$PC_{61}BM$ that absorbs photons up to 1000 nm. The detectivity of the NIR photodetector reaches as high as over 10^{13} Jones. Furthermore, the NIR photodetector is double-side responsive to incident light, either from the bottom or the top electrode, since the top tp-CP electrode shows similar transparency as the bottom indium-tin oxide electrode.

Key words: low dark current; NIR-OPDs; doping active layer; tp-CP electrode; highly transparent; double-side responsive

Introduction

Organic photodetectors (OPDs) as promising candidates for image sensors, digital photography, optical communication and environmental monitoring have received tremendous attention from both academy and industry.[1-7] The reasons are mainly owing to their brilliant merits of low cost, light weight, solution-processible, large-area detection and mechanical flexibility.[8-13] In addition, the absorption coefficient of many organic materials ($>10^5$ cm^{-1}) at wavelength above 700 nm, which are significantly higher than the corresponding values for silicon ($<10^3$ cm^{-1} above 700 nm), facilitate the OPDs to obtain the higher sensor sensitivity in the near-infrared (NIR) range.[14]

Typically, OPDs operate in photovoltaic[15-18] or photoconductive mode[19-23]. Photovoltaic-mode OPDs are of particular interest due to low operating voltage and faster response. It is well known that dark current is a critical parameter in photovoltaic-mode OPDs. Dark current is the source noise in restricting the sensitivity of the OPD device. In addition, higher dark current means higher recombination losses and higher power consumption.[24] To realize high performance NIR-OPD, achieving low dark current plays the crucial role. Previous endeavors to reduce the dark current are generally focused on inserting blocking layers or the thickness modulation of the active layer.[15, 25-27] In these devices, vacuum-deposited metals are used as the top electrodes. However, several groups have reported that metals would diffuse into pre-deposited organic semiconductor layers during the thermal deposition in high vacuum that significantly influences the performance of semiconductor devices.[28-30] For examples, Hirose and co-workers reported that metals (indium,

aluminum, silver and gold) will diffuse into 3,4,9,10-perylenetetracarboxylic dianhydride (PTCDA) films.[28] Pierre and co-workers obtained higher dark current density of the OPDs with vacuum-deposited metal electrodes that were ascribed to the diffusion of evaporated metal into the active layer.[29] To prevent the inter-diffusion between semiconductor and metals, Nowicki proposed titanium-tungsten or tungsten as thin film 'diffusion barriers' to prevent the interdiffusion between gold and silicon.[30]

In this work, we introduce a transfer-printed conducting polymer (tp-CP) poly(3,4-ethylenedioxythiophene):poly(styrene sulfonate) (PEDOT:PSS) top electrode[31] to realize highly efficient and easy-to-process NIR-OPD. The device structure is shown in Figure 1a. Our devices with the tp-CP electrode tactfully circumvent the semiconductor-metal interdiffusion problem. The devices exhibit significantly low dark current density (3.0 nA/cm^2 at -0.2 V) even without the hole or electron blocking layers. Furthermore, our OPD devices achieve double-side response and thus detect light from different incident directions owing to the high transmittance of PEDOT:PSS electrode. A high EQE of 48% at 850 nm is achieved when illuminated from the bottom electrode. A comparable EQE of 46% is obtained when illuminated from the top electrode. The detectivity (D^*) of the OPD device with the tp-CP electrode reaches 10^{13} Jones at -0.2 V that is nearly two orders of magnitude higher than that of the device with vacuum-deposited metal electrodes.

Experimental Section

Device fabrication: Indium tin oxide (ITO) glass substrates (CSG Holding Co. Ltd., Shenzhen) were cleaned in sequential ultrasonic baths of detergent in deionized water, deionized water, acetone and 2-propanol. The substrates were blown dry by nitrogen flow and then transferred to a N_2-fulled glovebox. Then ITO substrates were modified by spin coating a thin layer of polyethylenimine ethoxylated (PEIE, Sigma-Aldrich) at 5000 rpm for 1 min from a 2-propanol soluiton (0.1 wt.% of PEIE) that has been proved to effective reduce the work function of electrodes.[32] Then the substrates were thermal annealed at 100 °C for 5 min. After that, the low-bandgap active layer of PMDPP3T (synthesized as reported before[33]):$PC_{61}BM$ (1:3, weight ratio) was prepared by spin-coating from a solution with the total concentration of 20 mg ml^{-1} in a mixed solvent of chloroform and o-dichlorobenzene (o-DCB) (4:1, volume ratio) on glass/ITO/PEIE substrates at 1000 rpm for 1 min. The active layer was pumped for 10 min in the antechamber of the glove box and the thickness was measured to be 150 nm. After that, the tp-CP electrode was prepared on top of the active layer via transfer-printing method as we reported previously for solar cells.[34, 35] The schematic drawing of the transfer-printing procedure is shown in Fig. S1 of the supporting information. First of all, a piece of polydimethylsioxane (PDMS) was adhered on a clean glass substrate and was exposed to oxygen plasma for 50 s to tune its surface hydrophilicity. After that, high-conductivity of PEDOT:PSS PH1000 (Heraeus) formulation with 5 wt.% ethylene glycol (Sigma-Aldrich) and 0.1 wt.% surfactant (superwet-304, SurfyChem) was spin coated onto the PDMS at 1000 rpm for 1 min and dried in air for 6 min at 55% humidity. The PDMS

with PH1000 was cut into finger-shapes electrode. Before the PEDOT:PSS film transfer, substrates with the samples of glass/ITO/PEIE/PMDPP3T:$PC_{61}BM$ were exposed to a flash of oxygen plasma for about 5 s. Then, the PH1000 on top of PDMS was transferred onto the glass/ITO/PEIE/PMDPP3T:$PC_{61}BM$ with PH1000 contacting the photoactive layer. Finally, the top PDMS was slowly peeled off and the top electrode was left on the active layer to finish the fabrication of tp-CP electrode. For comparison, reference devices with MoO_3/Ag electrode were also fabricated where the electrode was deposited using Mini-spectros (Kurt J. Lesker) system at a base pressure of 2×10^{-7} Torr.

Film and device characterization: The transmittance of the ITO electrode and tp-CP electrode were measured on was conducted on a Spectrophotometer (UV-3600, Shimadzu Scientific Instruments). The *J-V* characteristics were measured inside a N_2-fillerd glove box by using a using a Keithley 2400 source meter controlled by a LabVIEW program in the dark and under illumination (AM 1.5, 100 mW cm^{-2}). Photodetector performance was measured using an Agilent B1500A semiconductor characterization system. The device was further covered with an aluminum cap to provide optical shielding. Monochromatic light-emitting diodes controlled by a functional generator (Agilent 33210A) were used as the light source. Light intensity was calibrated using a silicon photodetector (Newport 818-UV).

Results and discussions

Figure 1a shows the device structure of the as-prepared organic photodetector where the top electrode is prepared by transfer-printing technique. The delamination of the transfer

medium from the tp-CP electrode is also shown in Figure 1a. The active layer used in the NIR-OPD is PMDPP3T and $PC_{61}BM$ (Chemical structure is shown in Figure 1b). The PMDPP3T absorbs in the long-wavelength region up to 1000 nm that is a nice candidate for NIR photodetectors. The PMDPP3T has also been demonstrated as a very efficient donor material used in organic photovoltaics for both single-junction structure as well as tandem solar cells.[33, 36, 37] The mixture of PMDPP3T:$PC_{61}BM$ exhibits efficient charge transfer, separation and transport. Furthermore, the DPP-based polymer exhibits good air-stability and morphology stability. The processing additive such as 1,8-diiodooctane (DIO) is not required during the processing. It has been known that the removal of the DIO additive is critical to the solar cell performance. The high-vacuum pumping or solvent (such as methanol) washing has been demonstrated to be able to effectively remove the DIO additive.[38] Here, the PMDPP3T:$PC_{61}BM$ mixture doesn't require the additive of DIO, and displays good air stability. The active layer is potentially compatible with the solution-processed tp-CP top electrode in air that is without the high-vacuum pumping procedure. With PEIE-modified ITO as the bottom electrode, the energy level of each layer is shown in Figure 1c that indicates the potential efficient charge collection in the device. For comparison, devices with thermally vacuum-deposited MoO_3/Ag electrodes are also fabricated. The two types of the devices are denoted as OPD A and OPD B:

OPD A: glass/ITO/PEIE/PMDPP3T:$PC_{61}BM$/PEDOT:PSS.

OPD B: glass/ITO/PEIE/PMDPP3T:$PC_{61}BM$/MoO_3/Ag.

Figure 2 shows the *J-V* characteristics of the two types of devices in the dark and under 100 mW/cm^2 AM 1.5 illumination. Under illumination, the OPD A with the tp-CP electrode exhibits a short-circuit current density (J_{SC}) of 10.1 mA/cm^2, an open-circuit voltage (V_{OC}) of 0.6 V, a fill factor (FF) of 35.0% and the photovoltaic power conversion efficiency of 2.1%. For comparison, the reference device (OPD B) with MoO_3/Ag electrode displays a J_{SC} of 13.2 mA/cm^2, a V_{OC} of 0.63 V, FF of 55.7% and the PCE of 4.7%. The lower J_{SC} of the OPD A is related to the lack of the back light reflector. The poorer V_{OC} and FF might be associated to the larger sheet resistance of the tp-CP electrode (200 ohm/sq) than the MoO_3/Ag (< 1 ohm/sq), and the interface contact between the active layer and the top electrode because of the different energy levels of tp-CP electrode (work function: 4.9 eV) [32] and the MoO_3/Ag (conduction band: 6.7 eV, valence band: 9.7 eV). [39]

For the application as a photodetector, it is inspiring that the OPD A with the tp-CP displays much lower reverse dark current than the device B. The dark current density of OPD A is 2.98 $\times 10^{-9}$ A/cm^2 at a reverse bias of -0.2 V, which is over two orders of magnitude lower than that of OPD B (5.99 $\times 10^{-6}$ A/cm^2 at -0.2 V). As shown Figure 2a, the current under illumination of the OPDs (photovoltaic-mode) do not significant change when the reverse bias from 0 to -1 V, unlike previous reported photoconductive-mode OPDs whose EQE significantly changes as function of reverse bias. However, the dark current increases when the reverse bias becomes higher and leads to lower detectivity. Here, we calculate the detectivity of the OPDs at -0.2 V. The high reverse dark current of the OPD B is ascribed to the diffusion of the metal electrode (MoO_3/Ag) into the organic active layer during the

thermal evaporation.[29] Instead, the transfer-printing is a non-invasive method for the active layer and to provide a defect-free contact.[40] The tp-CP electrode is processed from water-based dispersion. It is difficult to diffuse into the hydrophobic active layer. Therefore, the device with the tp-CP electrode displays very low reverse dark current, while keeping comparable responsivity to the device with MoO_3/Ag electrode under illumination. It proves the effectiveness of tp-CP top electrode for the efficient OPDs. We have also fabricated device with MoO_3/PEDOT:PSS electrode. The device displays high reverse dark current (as shown in Fig. S2) that is comparable to the reference device with MoO_3/Ag electrode. This implies the possible migration of MoO_3 into the active layer during the thermal deposition.

Additionally, the device of OPD A demonstrates characteristic of double-side responsive to the incident light as the arrows denote in Figure 1a. The tp-CP electrode shows similar transmittance to the ITO electrode. The transmittance of the both electrodes is around 80% in the spectral region of 400 – 1100 nm as shown in Figure 3a. When light illuminated from the ITO electrode side and tp-CP electrode side, the device of OPD A exhibits similar EQE (Figure 3b). The EQE is 48% at 850 nm illuminated from ITO electrode while 46% illuminated from polymer electrode. It can also be observed that the photodetector is responsive up to 1000 nm from the EQE spectra with a peak value at 850 nm.

Responsivity (R) and detectivity (D^*) are the important parameters to evaluate the performance of photodetectors. Responsivity is defined as the ratio of photo-generated current to incident-light intensity.

$$R = J_{ph}/P_{in} \qquad (1)$$

Where J_{ph} is the photo-generated current density and P_{in} is the incident-light intensity density. Thus, R is calculated using Eq. 1 to be 0.37 A/W at 850 nm when light incidence from ITO bottom electrode and R is 0.35 A/W at 850 nm when light incidence from tp-CP top electrode with light intensity of 0.31 mW/cm^2 at -0.2V. Assuming that shot noise due to the dark current dominates total noise current of the OPDs, the D^* can be estimated as:[41]

$$D^* = R/(2qJ_d)^{\frac{1}{2}} = (J_{ph}/P_{in})(2qJ_d)^{\frac{1}{2}} \qquad (2)$$

Where R is the responsivity; q is the absolute value of electron charge (1.6×10^{-19} Coulombs); J_d is the dark current density; J_{ph} is the photo-generated current density and P_{in} is the incident-light intensity density under its dedicated wavelength. Based on the Equation 2, the D^* of OPD A is calculated to be $D^* = 1.23 \times 10^{13}$ Jones at -0.2 V when light incidence from the side of ITO bottom electrode (Figure 4a), while the reference device of OPD B shows a nearly two orders of magnitude lower D^* of 2.96×10^{11} Jones.

Another figure of merit for photodetectors is the linear dynamic range (LDR). LDR is defined as [42]:

$$\mathrm{LDR} = 20\log\left(\frac{J_{upper}}{J_{\mathrm{lower}}}\right) = 20\log\left(\frac{L_{upper}}{L_{\mathrm{lower}}}\right)$$

Where J and L denote the current density and input light irradiance respectively. The upper limit of the LDR is given by the current value that deviates from linearity, and is defined by the slower carrier transit time. The lower limit of the LDR is governed by the detection limit of our equipment. The LDR we measured for OPD A is 120 dB (Fig. 4b), which is comparable to the LDR for Si photodetector.

Conclusions

In conclusion, we have reported high-performance a NIR-OPD by employing tp-CP PEDOT:PSS as the top electrode to replace the commonly used thermally vacuum-deposited metal oxides/metals. The use of tp-CP to fabricate top electrode not only significantly lower the dark current density by over two orders of magnitude of the photodetectors than photodetector with vacuum-deposited metals as the top electrode., but also greatly simplifies the fabrication process of the OPD devices without the need of the high-vacuum deposition or inserting blocking layers. The active layer containing low-band gap DPP-based material enables the photodetector to respond towards 1000 nm. This is also the first example of the solution-processed polymer electrodes used in the DPP-based polymer optoelectronic devices. The PEDOT:PSS polymer electrode is highly transparent and thus the NIR photodetectors are semitransparent and able to respond light from different incident directions. Therefore, the easy fabrication, high performance and double-side responsive property of the NIR photodetectors enables their promising for broad sensing applications. Our results demonstrate that tp-CP PEDOT:PSS as top electrode is an effective means of fabricating high-efficiency OPD and bring us new perspectives to suppress the dark current of OPD.

Acknowledgements

We thank Kai Zeng and Hui Deng for the assistance on the measurement under different light intensity density. The work is supported by the Recruitment Program of Global

Youth Experts, the National Natural Science Foundation of China (Grant No. 51403071), the Fundamental Research Funds for the Central Universities, HUST (Grant No. 2014YQ013).

References

1. T. N. Ng, W. S. Wong, M. L. Chabinyc, S. Sambandan and R. A. Street, *Appl.Phys. Lett.*, 2008, **92**, 213303.
2. S. Nau, C. Wolf, S. Sax and E. J. List-Kratochvil, *Adv. Mater.*, 2015, **27**, 1048-1052.
3. A. Armin, R. D. Jansen-van Vuuren, N. Kopidakis, P. L. Burn and P. Meredith, *Nat. Commun.*, 2015, **6**, 6343.
4. I. K. Kim, B. N. Pal, M. Ullah, P. L. Burn, S.-C. Lo, P. Meredith and E. B. Namdas, *Adv. Opt. Mater.*, 2015, **3**, 50-56.
5. L. Chen, L. Huang, D. Yang, S. Ma, X. Zhou, J. Zhang, G. Tu and C. Li, *J. Mater. Chem. A*, 2014, **2**, 2657.
6. A. Armin, M. Hambsch, I. K. Kim, P. L. Burn, P. Meredith and E. B. Namdas, *Laser Photonics Rev.*, 2014, **8**, 924-932.
7. X. Gong, M. Tong, Y. Xia, W. Cai, J. S. Moon, Y. Cao, G. Yu, C.-L. Shieh, B. Nilsson and A. J. Heeger, *Science*, 2009, **325**, 1665-1667.
8. T. Rauch, M. Böberl, S. F. Tedde, J. Fürst, M. V. Kovalenko, G. Hesser, U. Lemmer, W. Heiss and O. Hayden, *Nat. Photonics*, 2009, **3**, 332-336.
9. M. S. Arnold, J. D. Zimmerman, C. K. Renshaw, X. Xu, R. R. Lunt, C. M. Austin and S. R. Forrest, *Nano Lett.*, 2009, **9**, 3354-3358.
10. P. E. Keivanidis, P. K. H. Ho, R. H. Friend and N. C. Greenham, *Adv.Funct.Mater.*, 2010, **20**, 3895-3903.
11. Y. Yao, Y. Liang, V. Shrotriya, S. Xiao, L. Yu and Y. Yang, *Adv.Mater.*, 2007, **19**, 3979-3983.
12. H. Zhang, S. Jenatsch, J. De Jonghe, F. Nüesch, R. Steim, A. C. Véron and R. Hany, *Sci. Rep.*, 2015, **5**, 9439.
13. I. K. Kim, X. Li, M. Ullah, P. E. Shaw, R. Wawrzinek, E. B. Namdas and S. C. Lo, *Adv. Mater.*, 2015, DOI: 10.1002/adma.201502936.
14. D. Y. K. Chi Hang Cheung, Jegadesan Subbiah, Chad M. Amb, and a. F. S. John R. Reynolds, *Trans. Electron. Devices*, 2014, **61**.
15. L. Zhang, T. Yang, L. Shen, Y. Fang, L. Dang, N. Zhou, X. Guo, Z. Hong, Y. Yang, H. Wu, J. Huang and Y. Liang, *Adv. Mater.*, 2015, DOI: 10.1002/adma.201502267.
16. D. Yang, X. Zhou and D. Ma, *Org. Electron.*, 2013, **14**, 3019-3023.
17. D. Yang and D. Ma, *J. Mater. Chem. C*, 2013, **1**, 2054.
18. X. Hu, K. Wang, C. Liu, T. Meng, Y. Dong, S. Liu, F. Huang, X. Gong and Y. Cao, *J. Mater. Chem. C*, 2014, **2**, 9592-9598.

19. L. Li, F. Zhang, W. Wang, Q. An, J. Wang, Q. Sun and M. Zhang, *ACS Appl. Mater. Interfaces*, 2015, **7**, 5890-5897.
20. L. Li, F. Zhang, W. Wang, Y. Fang and J. Huang, *Physical chemistry chemical physics : PCCP*, 2015, **17**, 30712-30720.
21. W. Wang, F. Zhang, L. Li, M. Zhang, Q. An, J. Wang and Q. Sun, *J. Mater. Chem. C*, 2015, **3**, 7386-7393.
22. L. Shen, Y. Fang, Q. Dong, Z. Xiao and J. Huang, *Appl. Phys. Lett.*, 2015, **106**, 023301.
23. H. Wei, Y. Fang, Y. Yuan, L. Shen and J. Huang, *Adv. Mater.*, 2015, **27**, 4975-4981.
24. M. Binda, A. Iacchetti, D. Natali, L. Beverina, M. Sassi and M. Sampietro, *Appl. Phys. Lett.*, 2011, **98**, 073303.
25. F. Guo, Z. Xiao and J. Huang, *Adv. Opt. Mater.*, 2013, **1**, 289-294.
26. D.-S. Leem, K.-H. Lee, Y.-N. Kwon, D.-J. Yun, K.-B. Park, S.-J. Lim, K.-S. Kim, Y. W. Jin and S. Lee, *Org. Electron.*, 2015, **24**, 176-181.
27. X. Liu, J. Zhou, J. Zheng, M. L. Becker and X. Gong, *Nanoscale*, 2013, **5**, 12474-12479.
28. Y. Hirose, A. Kahn, V. Aristov, P. Soukiassian, V. Bulovic and S. R. Forrest, *Phys.Rev. B*, 1996, **54**, 13748-13758.
29. A. Pierre, I. Deckman, P. B. Lechene and A. C. Arias, *Adv. Mater.*, 2015, DOI: 10.1002/adma.201502238.
30. R. Nowicki, *Gold Bull.*, 1982, **15**, 21-24.
31. Y. Zhou, T. M. Khan, J. W. Shim, A. Dindar, C. Fuentes-Hernandez and B. Kippelen, *J. Mater. Chem. A*, 2014, **2**, 3492.
32. Y. Zhou, C. Fuentes-Hernandez, J. Shim, J. Meyer, A. J. Giordano, H. Li, P. Winget, T. Papadopoulos, H. Cheun, J. Kim, M. Fenoll, A. Dindar, W. Haske, E. Najafabadi, T. M. Khan, H. Sojoudi, S. Barlow, S. Graham, J. L. Bredas, S. R. Marder, A. Kahn and B. Kippelen, *Science*, 2012, **336**, 327-332.
33. W. Li, A. Furlan, K. H. Hendriks, M. M. Wienk and R. A. Janssen, *J. Am. Chem. Soc.*, 2013, **135**, 5529-5532.
34. F. Jiang, T. Liu, S. Zeng, Q. Zhao, X. Min, Z. Li, J. Tong, W. Meng, S. Xiong and Y. Zhou, *Opt. Express*, 2015, **23**, A83-A91.
35. J. Tong, S. Xiong, Z. Li, F. Jiang, L. Mao, W. Meng and Y. Zhou, *Appl.Phys. Lett.*, 2015, **106**, 053306.
36. A. R. b. M. Yusoff, D. Kim, H. P. Kim, F. K. Shneider, W. J. da Silva and J. Jang, *Energy Environ. Sci.*, 2015, **8**, 303-316.
37. O. Adebanjo, P. P. Maharjan, P. Adhikary, M. Wang, S. Yang and Q. Qiao, *Energy Enviro. Sci.*, 2013, **6**, 3150.
38. L. Ye, Y. Jing, X. Guo, H. Sun, S. Zhang, M. Zhang, L. Huo and J. Hou, *J. Phys. Chem. C*, 2013, **117**, 14920-14928.
39. M. Kroger, S. Hamwi, J. Meyer, T. Riedl, W. Kowalsky and A. Kahn, *Appl. Phys. Lett.*, 2009, **95**, 123301.
40. D. Gupta, M. M. Wienk and R. A. J. Janssen, *Adv. Energy Mater.*, 2013, **3**, 782-787.
41. X. Gong, M. H. Tong, S. H. Park, M. Liu, A. Jen and A. J. Heeger, *Sensors (Basel)*, 2010, **10**, 6488-6496.
42. Q. Lin, A. Armin, D. M. Lyons, P. L. Burn and P. Meredith, *Adv. Mater.*, 2015, **27**, 2060-2064.

Fig. 1(a) Device structure of the double-side responsive near-infareard photodetector: glass/ITO/PEIE/PMDPP3T:$PC_{61}BM$/PEDOT:PSS; (b) Chemical structures of PMDPP3T and $PC_{61}BM$; (c) Energy diagram of each layer used in the photodetector.

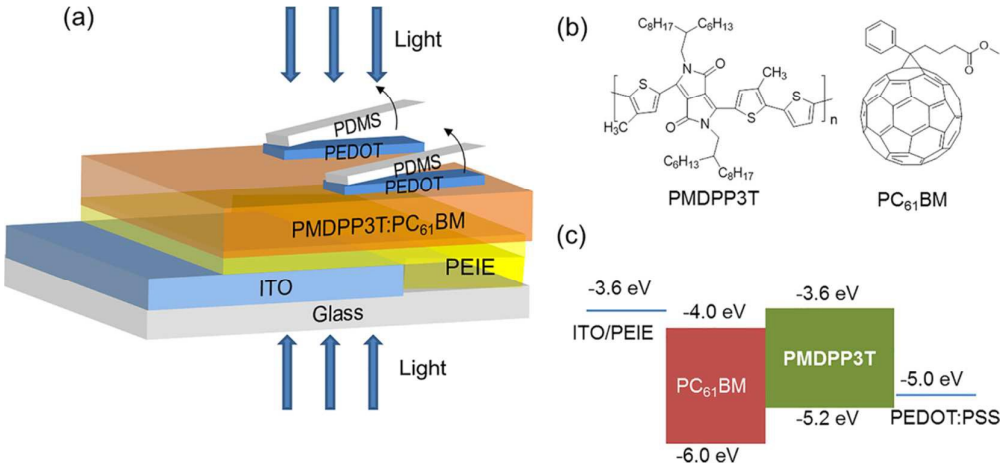

Fig. 2 (a) *J-V* characteristics of glass/ITO/PEIE/PMDPP3T:$PC_{61}BM$/PEDOT:PSS in the dark and under simulated 1 sun illumination where the PEDOT:PSS electrode is prepared via transfer-printing method. The red dot line is the *J-V* characteristics curve of light incidence from PEDOT:PSS polymer top electrode and the green triangle line is the *J-V* characteristics curve of light incidence from ITO bottom electrode. (b) *J-V* characteristics of glass/ITO/PEIE/PMDPP3T:$PC_{61}BM$/MoO_3/Ag where MoO_3/Ag is prepared by thermal deposition in high vacuum.

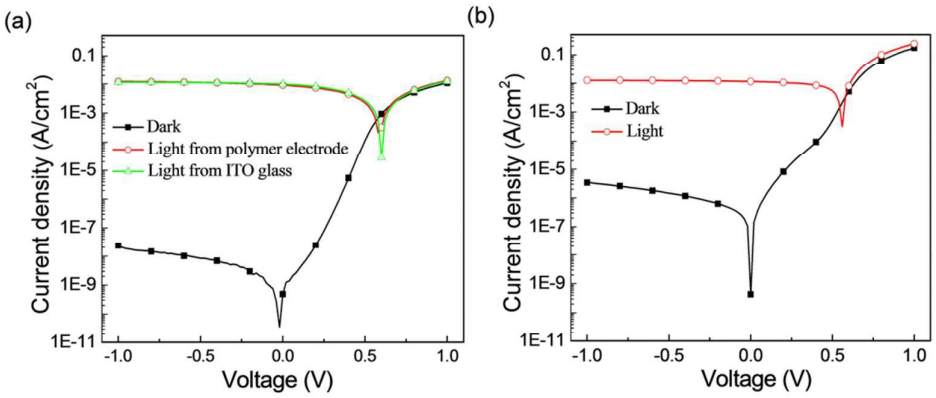

Fig. 3 (a) Transmittance of the ITO bottom electrode and the PEDOT:PSS polymer top electrode. The blue dot line is the transmittance of PEDOT:PSS polymer top electrode and the red triangle line is the transmittance of ITO bottom electrode. (b) EQE of light from different incident directions.. The blue dot line is the EQE of light incidence from PEDOT: PSS polymer top electrode and the red triangle line is the EQE of light incidence from ITO bottom electrode.

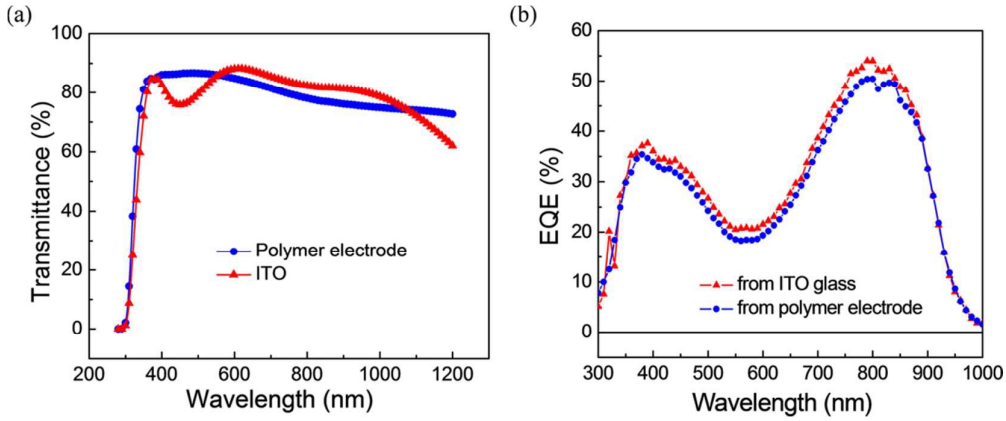

Fig. 4 (a) The detectivities of the OPD A (glass/ITO/PEIE/PMDPP3T:$PC_{61}BM$/PEDOT:PSS) versus the wavelength. The blue line is the detectivities of light incidence from PEDOT:PSS polymer top electrode and the red line is the detectivities of light incidence from ITO bottom electrode. (b) Current density of the OPD as a function of light intensity at 850 nm.

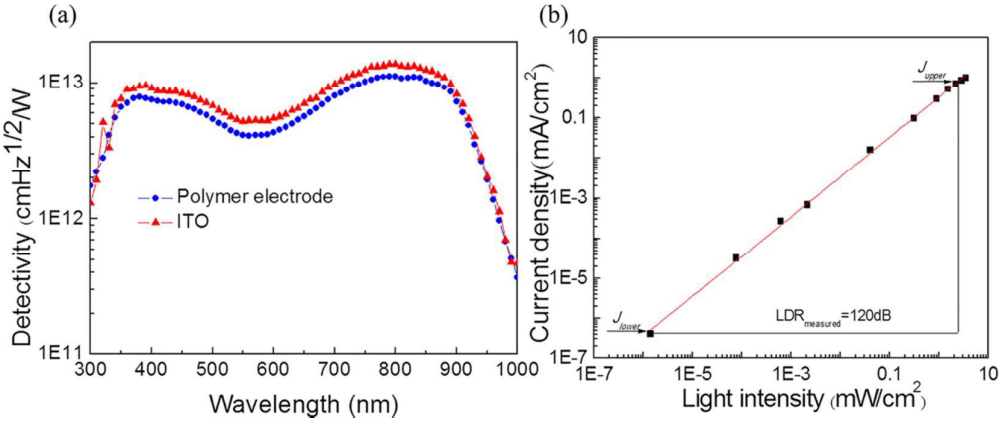

Graphical Abstract

Transfer-printed conducting polymer (tp-CP) is employed as the top electrode for near-infrared organic photodetectors. The photodetector exhibits a high detectivity of 10^{13} Jones that is two orders of magnitude higher than that of the photodetector with MoO_3/Ag electrode. Furthermore, The photodetector is double-side responsive.